Mechanism of Ni-catalyzed Photochemical Halogen Atom-Mediated C(sp^3)–H Arylation

Alexander Q. Cusumano, Braden C. Chaffin, and Abigail G. Doyle*

*Ni catalysis, metallaphotoredox catalysis, mechanistic study, C–H activation*

ABSTRACT: Within the context of Ni photoredox catalysis, halogen atom photoelimination from Ni has emerged as a fruitful strategy for enabling hydrogen atom transfer (HAT)-mediated C(sp^3)-H functionalization within the context of Ni photoredox catalysis. Despite the numerous synthetic transformations invoking this paradigm, a unified mechanistic hypothesis that is consistent with experimental findings on the catalytic systems and accounts for halogen radical formation and facile C(sp^2)–C(sp^3) bond formation remains elusive. We employ kinetic analysis, organometallic synthesis, and computational investigations to decipher the mechanism of a prototypical Ni-catalyzed photochemical C(sp^3)–H arylation reaction. Our findings revise the previous mechanistic proposals, first by examining the relevance of SET and EnT processes from Ni intermediates relevant to the HAT-based arylation reaction. Our investigation highlights the ability for blue light to promote efficient Ni–C(sp^2) bond homolysis from cationic Ni^{III} and C(sp^2)–C(sp^3) reductive elimination from bipyridyl Ni^{II} complexes. However interesting, the rates and selectivities of these processes do not account for the productive catalytic pathway. Instead, our studies support a mechanism that involves halogen atom evolution from in situ generated Ni^{II} dihalide intermediates, radical capture by a Ni^{II}(aryl)(halide) resting state, and a key C–C bond formation from Ni^{III}. Oxidative addition to Ni^{I}, as opposed to Ni^{0}, and rapid Ni^{III}/Ni^{I} comproportionation play key roles in this process. The findings presented herein offer fundamental insight into the reactivity of Ni in the broader context of catalysis.

INTRODUCTION

The advent of Ni metallaphotoredox catalysis has facilitated novel approaches to forge challenging C–C and C–heteroatom bonds.[1] Recently, interfacing hydrogen atom transfer (HAT) processes within Ni metallaphotoredox catalysis has emerged as a salient strategy to generate highly reactive organic radicals in situ from aliphatic C–H coupling partners.[2] The capture of these radicals by a Ni catalyst, and subsequent C–C/X bond-formation, enables a broader paradigm of direct C(sp^3)–H cross-coupling (Figure 1A).[3]

In 2016, initial reports by the Doyle[4] and Molander[5] groups showcased the Ni-catalyzed photochemical C(sp^3)–H arylation of cyclic and acyclic ethers using in situ-generated halogen atom radicals for HAT (Figure 1B). The Doyle group was inspired by reports from the Nocera laboratory demonstrating the ability of Ni^{III} trihalide complexes to undergo blue light-induced photoelimination of free halogen atoms.[6] Doyle and coworkers envisioned the catalytic generation of Ni^{III} halides from single electron oxidation of Ni^{II} by an excited-state Ir^{III} photocatalyst (**1***). Ni^{III}–X photolysis then ensues, with the resultant free halogen atoms serving as a powerful HAT reagent (Figure 1B). Meanwhile, the Molander group posited an analogous process with halogen atom ejection directly from Ni^{II} aryl halide intermediates upon triplet energy transfer (^{3}EnT) from a similar photocatalyst (**2**).[5] While building upon distinct hypotheses, both groups successfully developed C(sp^3)–H cross-coupling reactions employing aryl bromide and chloride electrophiles – ultimately under nearly identical reaction conditions (4,4'-di-*tert*-butyl-2,2'-bipyridine ligands (*^{t}-Bu*bpy), potassium phosphate bases, and similar photocatalysts (**1** and **2**)). Since these initial disclosures, numerous reports have employed and built upon these principles to enable novel synthetic transformations.[7]
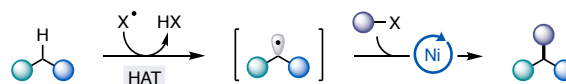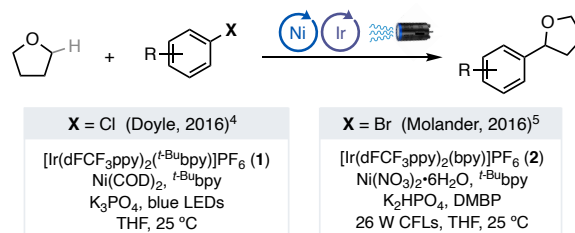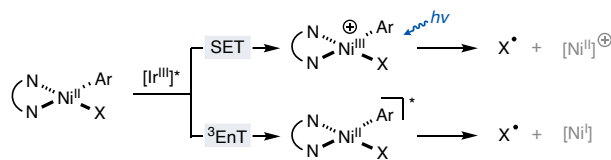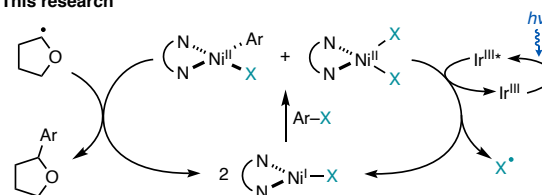

Figure 1. (A) C–H functionalization via HAT in Ni photocatalysis. (B) Seminal reports in the C(sp^3)–H arylation of cyclic and acyclic ethers. (C) This research.

Despite these developments, a generalized mechanism for halogen atom-mediated Ni-catalyzed photochemical C(sp³)–H cross-couplings has yet to be established. Building upon recent insights in photochemistry of bipyridine Ni organometallics, we report a comprehensive mechanistic study of a prototypical Ni-catalyzed photochemical C(sp³)–H arylation reaction (Figure 1C). The SET- and ³EnT-based mechanistic hypotheses first proposed by Doyle and Molander represented the natural starting point for our investigations. Our studies of SET-based mechanisms uncovered the ability of cationic Ni^III to undergo rapid blue light-induced Ni–C(sp²) bond homolysis, even at cryogenic temperatures. Meanwhile, experiments geared toward probing ³EnT pathways ultimately revealed ³MLCT states of Ni^II(aryl)(alkyl) complexes, accessed by direct irradiation or ³EnT, efficiently promote C–C bond formation via reductive elimination.[8,9]

Nevertheless, we find that neither of these interesting chemistries can account for the reactivity of the catalytic system. Instead, we propose a new mechanistic hypothesis involving halogen atom evolution from in situ generated Ni^II dihalide intermediates, radical capture by a Ni^II(aryl)(halide) resting state, and C–C bond formation through reductive elimination at Ni^III. Recent studies highlight the ability of Ni^I to readily undergo oxidative addition with both aryl chlorides and bromides.[10,11] Accordingly, facile oxidative addition of aryl halides to Ni^I, rather than Ni^0, and rapid downstream Ni^III/Ni^I comproportionation play key roles in the mechanism. Ni–X bond homolysis from an excited-sate of the Ni^II dihalide product of this process ultimately serves as the halogen atom source enabling HAT. These results are in accord with recent reports that find similar Ir^III photocatalysts preferentially undergo ³EnT with bipyridine Ni^II complexes rather than SET.[8,9,12] These findings highlight the ability of Ni to generate highly reactive intermediates and forge challenging bonds in the broader context of catalysis.

RESULTS AND DISCUSSION

Excited-state Ir^III photocatalysts (Ir^III*) (1* and 2*) may engage Ni in either SET or EnT processes. Both initial reports by Doyle and Molander propose accessing a common (^t-Bu bpy)Ni^II(aryl)(X) intermediate (X = Cl, Br) (3). However, this point is where the SET/EnT dichotomy led the hypotheses to diverge.

In the energy transfer-based mechanism put forth by Molander and coworkers, ³EnT from Ir^III* to (^t-Bu bpy)Ni^II(aryl)(X) (3) leads to a triplet excited-state of (3). This triggers Ni–X bond homolysis to afford a (^t-Bu bpy)Ni^I(aryl) intermediate (4) and a halogen atom (Figure 2, left).[5] Hydrogen atom transfer (HAT) to the free halogen atom from the tetrahydrofuran (THF) solvent produces radical intermediate 5. Recombination with Ni^I (4) affords a (^t-Bu bpy)Ni^II(aryl)(THF) complex (6), which liberates the cross-coupled product 8 upon reductive elimination and ligand exchange. Oxidative addition of the resultant Ni^0 (9) with the aryl halide electrophile (10) regenerates (^t-Bu bpy)Ni^II(aryl)(X) (3).

Alternatively, Doyle and coworkers hypothesized that the excited-state of [Ir(dF(CF₃)ppy)₂(^t-Bu bpy)]PF₆ (1) oxidizes Ni^II aryl halide intermediate 3 (Figure 2, right),[4] directly affording cationic Ni^III aryl halide complex 11. Efficient blue light-promoted halogen atom photoelimination from Ni^III trihalide and cationic Ni^III dihalide complexes has been demonstrated by the Nocera[6] and Mirica[13] groups. Accordingly, 11 would undergo reductive photolysis to afford cationic (^t-Bu bpy)Ni^II(aryl)⁺ intermediate 12 and a free halogen atom. An analogous HAT and recombination process yields (^t-Bu bpy)Ni^III(aryl)(THF)⁺ (13), which readily undergoes C–C bond forming reductive elimination. The redox cycle is completed by reduction of the cationic Ni^I product (14) to Ni^0, regenerating the Ir^III photocatalyst (1).

Given the proposed intermediacy of and diverged reactivity from (^t-Bu bpy)Ni^II(aryl)(X) complexes (3), we began by evaluating the role of these species in the productive C–H arylation reaction.
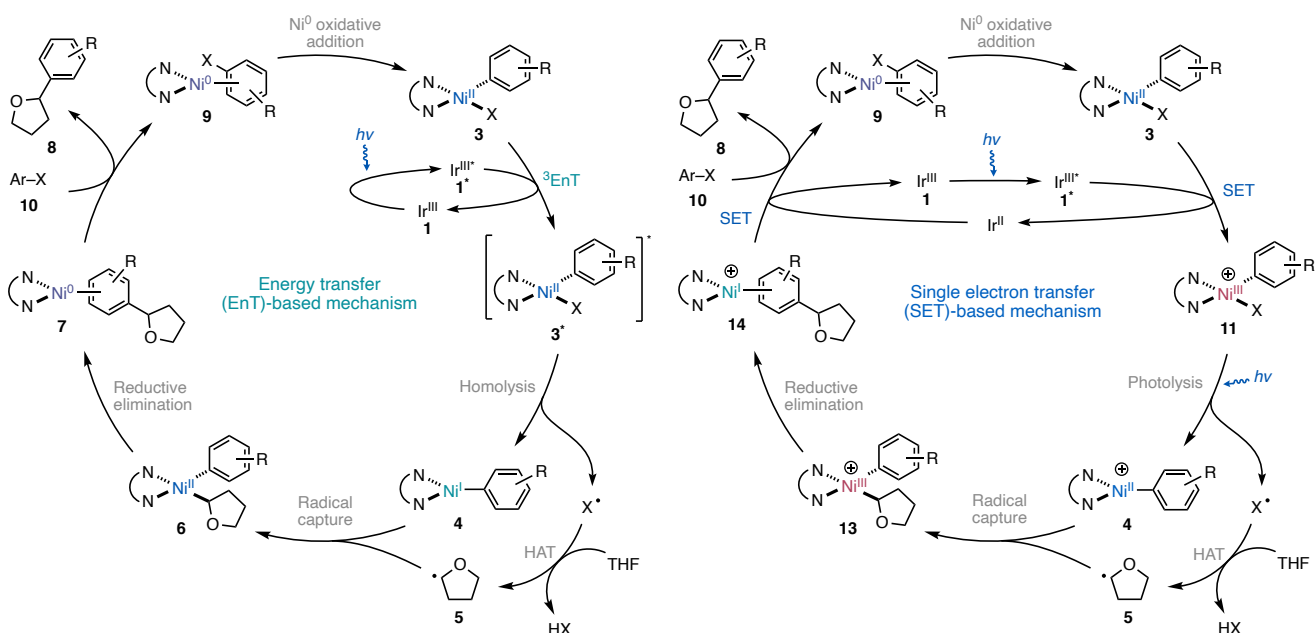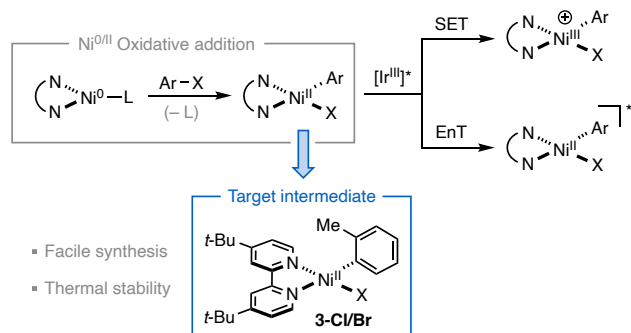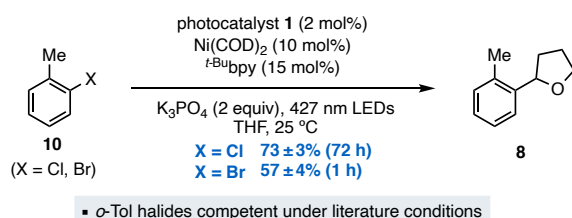

Figure 2. Representative triplet energy transfer (³EnT) (left) and single electron transfer (SET)-based (right) mechanisms for the C–H arylation of THF. In this study, R = 2-Me.
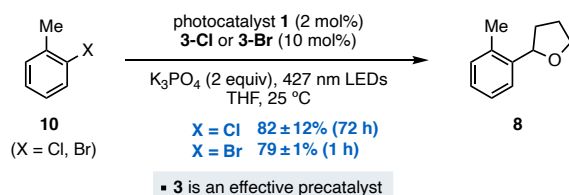
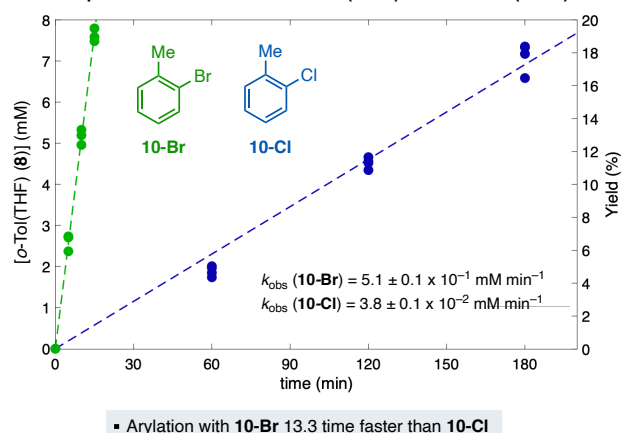**A. Representative common ($^{t\text{-Bu}}$bpy)Ni(aryl)(X) intermediate (X = Cl, Br)**

B. Literature reaction conditions with *o*-Tol halide electrophiles

photocatalyst **1** (2 mol%)
Ni(COD)$_2$ (10 mol%)
$^{t\text{-Bu}}$bpy (15 mol%)
―――――――――――――――
K$_3$PO$_4$ (2 equiv), 427 nm LEDs
THF, 25 °C

10
(X = Cl, Br)

X = Cl 73 ± 3% (72 h)
X = Br 57 ± 4% (1 h)

8

- *o*-Tol halides competent under literature conditions

C. Employing 3 as precatalyst with *o*-Tol halide electrophiles

photocatalyst **1** (2 mol%)
3-Cl or **3-Br** (10 mol%)
―――――――――――――――
K$_3$PO$_4$ (2 equiv), 427 nm LEDs
THF, 25 °C

10
(X = Cl, Br)

X = Cl 82 ± 12% (72 h)
X = Br 79 ± 1% (1 h)

8

- **3** is an effective precatalyst

D. Rate comparison between *o*-Tol chloride (10-Cl) and bromide (10-Br).

k_{obs} (**10-Br**) = 5.1 ± 0.1 x 10^{-1} mM·min^{-1}
k_{obs} (**10-Cl**) = 3.8 ± 0.1 x 10^{-2} mM·min^{-1}

- Arylation with **10-Br** 13.3 time faster than **10-Cl**

E. Linear dependence of reaction rate on LED lamp power
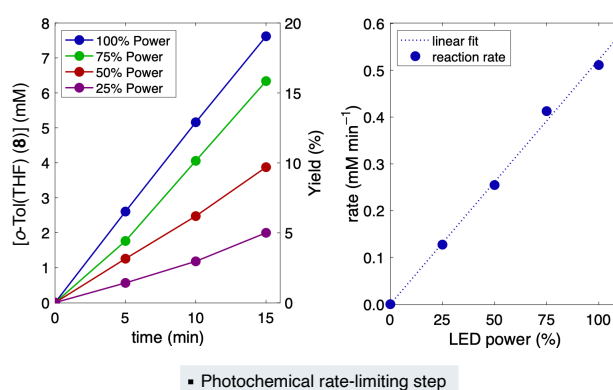
- Photochemical rate-limiting step

Figure 3. (A–C) Proposed role and competency of **3** in catalysis. (D) Global observed rates for the C–H arylation with **10-Cl/Br**. (E) Dependence of reaction rate on light power with **10-Br**. Reactions performed on 0.05 mM scale with dodecane as an internal standard (GC-FID yields). Errors reflect a 95% confidence interval.

Evaluation of ($^{t\text{-Bu}}$bpy)Ni^{II}(aryl)(halide) complexes as intermediates. Both original reports[4,5] demonstrate the compatibility of Ni^0 and Ni^{II} precatalyst, with preference for Ni^0(COD)$_2$ and Ni^{II}(NO$_3$)$_2$·6H$_2$O in the cross-couplings of aryl chlorides and bromides, respectively. Nevertheless, both mechanistic hypotheses invoke reactivity (either SET or ^{3}EnT) from a common ($^{t\text{-Bu}}$bpy)Ni^{II}(aryl)(X) intermediate (**3**). Hence, such **3** serves as a natural starting point from which to begin our investigations.

First, we sought to explore the catalytic competency of the proposed ($^{t\text{-Bu}}$bpy)Ni^{II}(aryl)(X) intermediates. *ortho*-Tolyl (*o*-Tol) halide derived complexes **3-Cl** and **3-Br** are ideal analogs due to their stability and straightforward preparation (Figure 3A). Moreover, under our representative reaction conditions with Ni^0(COD)$_2$, $^{t\text{-Bu}}$bpy, K$_3$PO$_4$, and photocatalyst **1**, the corresponding *o*-Tol chloride and bromide electrophiles (**10**) are competent substrates in the C–H arylation of THF, furnishing cross-coupled product **8** in 73% and 57% yield, respectively (Figure 3B). The ability of ($^{t\text{-Bu}}$bpy)Ni^{II}(*o*-Tol)(X) complexes (**3**) to promote cross-coupling in similar yields to the standard conditions suggests the Ni^{II} intermediates are not the products of irreversible catalyst deactivation (Figure 3C).

The conserved rate difference between aryl chloride and bromide substrates is noteworthy. Typical reaction times from aryl chlorides require upwards of 72 h to reach full conversion, while aryl bromides only require one hour. Initial rate studies find the rate of product formation from **10-Br** to be 13.3 times greater than that from **10-Cl** (Figure 3D). Initially, we posited this rate-difference may arise from a rate-limiting oxidative addition. However, variable time normalization analysis (VTNA)[14] studies with variable aryl halide concentration reveals no dependence of aryl halide on the global reaction rate (see SI). Moreover, k_{obs} is linearly dependent on LED power (Figure 3E), suggesting reaction rate is limited by a photochemical process, rather than a dark Ni$^{0/II}$ oxidative addition. Hence, the order-of-magnitude rate difference observed between aryl chlorides and bromides must be attributed to a different step in the mechanism (see later discussions).

Given a facile oxidative addition, a light-dependent reaction rate, and the catalytic competency of **3**, we hypothesized that photochemistry from a ($^{t\text{-Bu}}$bpy)Ni^{II}(*o*-Tol)(X) resting state is rate-limiting. To probe this, we sought to monitor the distribution of reaction components in situ by ^{19}F NMR, employing fluorine tagged *o*-Tol bromide **15** and its corresponding Ni^{II} complex **16** (Figure 4). The reaction mixture was subjected to standard reaction conditions for 20 minutes to reach approximately 30–50% conversion. ^{19}F NMR analysis reveals a 34% yield of the cross-coupled product (**17**) (corresponding to an effective catalyst TON of 3.4) with 77% of Ni remaining as **16**. No other

diamagnetic fluorine-labeled species were observed. While these experiments are consistent with a ($^{t\text{-Bu}}$bpy)Ni^{II}(o-Tol)(X) resting state, they do not preclude the possibility of an alternative on-cycle resting state with **3** serving as an off-cycle catalyst reservoir requiring light activation.

To further examine this hypothesis, we assessed the ability of the ($^{t\text{-Bu}}$bpy)Ni^{II}(o-Tol)(X) complexes (**3-Cl/Br**) to furnish a stoichiometric yield of cross-coupled product (**8**) in the absence of aryl halide, under otherwise identical catalytic conditions. Indeed, complexes **3-Cl** and **3-Br** afforded **8** in 16% and 21% yield, respectively (Figure 5A). We suspected the diminished yield may arise from comproportionation of a Ni^0 product with starting Ni^{II} (**3**) to yield Ni^{I} byproducts. Under the catalytic conditions, the relative excess of aryl halide and oxidative addition to Ni^0 would avoid this degradation process. As such, we subjected ($^{t\text{-Bu}}$bpy)Ni^{II}(o-Tol)(Br) (**3-Br**) to the standard reaction conditions for 20 min, but in the presence 10 equivalents of 4-bromobenzotrifluoride (**18**) as a sacrificial substrate (Figure 5B). Surprisingly, while 3.1 equivalents of **19** were formed (effective catalyst TON of 3.1), the o-Tol cross-coupled product (**8**) was not observed, rather **10-Br** was evolved in 64% yield. We then subjected the analogous ($^{t\text{-Bu}}$bpy)Ni^{II}(p-CF$_3$Ph)(Br) complex (**20**) to the standard reaction conditions in the presence of 10 equivalents of o-TolBr (**10-Br**). After 20 minutes, the inverse crossover experiment afforded one equivalent of the trifluoromethyl cross-coupled product (**19**) from one equivalent of **20** with only trace p-CF$_3$ electrophile (**18**) observed (Figure 5B).
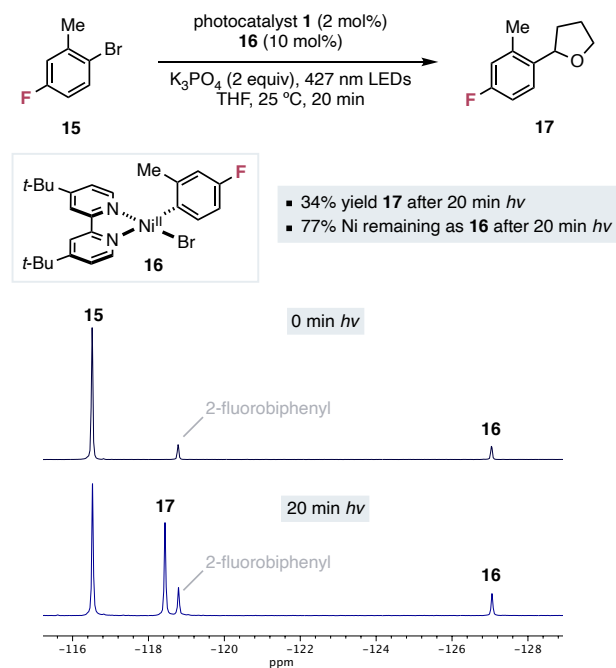

Figure 4. In situ reaction monitoring by ^{19}F NMR. Reaction performed on 0.05 mM scale with 2-fluorobiphenyl as an internal standard (^{19}F NMR yield).

These results suggest the reaction conditions support a background process involving light-induced aryl bromide reductive elimination from Ni^{II} (**3**) to Ni^0 (**9**) followed by a fast ground-state oxidative addition from 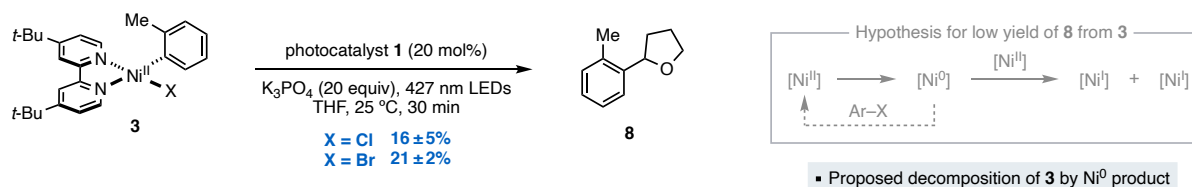Ni^0 (**9**) to regenerate **3** (Figure 5D). Aryl bromide ligand exchange can occur at this Ni^0 intermediate, allowing for the liberation of **10-Br** and formation of a new Ni^{II} aryl halide complex. Under such conditions, the relative rate of oxidative addition and concentration difference between o-Tol and p-CF$_3$-substituted electrophiles (**10-Br** and **18**) likely bear the greatest influence on intermediate product distribution. As this hypothetical process is orthogonal to productive catalysis, we sought to explore whether the aryl halide exchange persists in the absence of the THF coupling partner and base. Indeed, after only 5 minutes of 427 nm irradiation of **3-Br** in the presence of **18** (10 equiv) and photocatalyst **1** (10 mol%) in C$_6$D$_6$, 1.0 equivalent of **10-Br** and 95% yield of ($^{t\text{-Bu}}$bpy)Ni^{II}(p-CF$_3$Ph)(Br) **20** were afforded (Figure 5C). These results are in accord with a recent kinetic study of a Ni/Ir-photocatalyzed cross-electrophile coupling of aryl and alkyl bromides by Lloyd-Jones.[15] There, complex **20** was demonstrated to undergo aryl bromide cycling with ^{13}C-labeled **18**, ultimately achieving an even distribution between ^{13}**C-18** to ^{13}**C-20**.

We posited the excited-state photocatalyst (**1***) may undergo triplet energy transfer with **3-Br** to access triplet metal-to-ligand charge transfer (^{3}MLCT) states of **3-Br** (see SI for discussion). These states likely play a key role, as the effectively cationic Ni^{III} electronic configuration facilitates a spin-allowed C–X bond formation. These same states may be accessible through irradiation of **3-Br** in the absence of photocatalyst by directly targeting S$_0 \rightarrow ^1$MLCT transitions. Indeed, irradiation with the same 427 nm wavelength light promotes aryl halide exchange even in the absence of **1** (Figure 5C). This observation highlights that the photocatalyst is not required to engage in SET with **3-Br**, and a 3EnT process is likely at play.
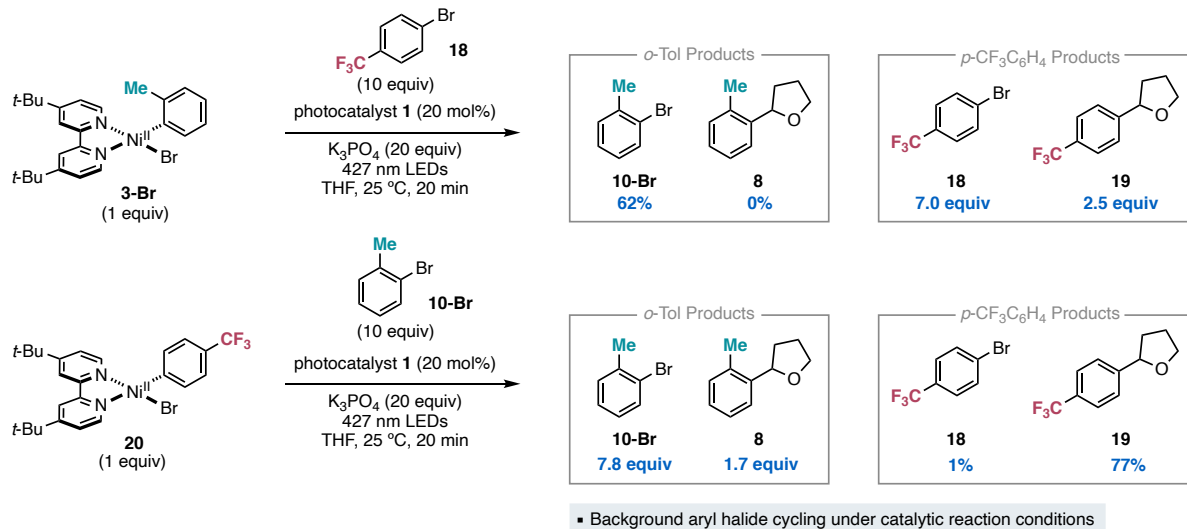
In summary, we find ($^{t\text{-Bu}}$bpy)Ni^{II}(aryl)(halide) complexes represent competent catalytic intermediates in the C–H arylation of THF. Kinetic studies suggest a photon flux-dependent rate-limiting process. Aryl halide oxidative addition is fast, and under photochemical conditions, reversible.[15] In situ ^{19}F NMR studies find ($^{t\text{-Bu}}$bpy)Ni^{II}(aryl)(halide) persist as a major Ni species during the reaction. Considering these data, we assign the ($^{t\text{-Bu}}$bpy)Ni^{II}(aryl)(halide) complex as a Ni catalyst resting state under the standard reaction. Hence, understanding the downstream reactivity from ($^{t\text{-Bu}}$bpy)Ni^{II}(aryl)(halide) complexes and the interplay of SET and EnT processes between these species and excited-state Ir is a critical next step in our investigation.

Evaluation of a SET-based mechanism. Key to the C–H arylation reaction is the generation of an organic radical coupling partner (**5**) by HAT with a halogen atom. Seminal reports by Nocera and coworkers showcase the ability of (L$_2$)Ni^{III}X$_3$ complexes (X = Cl, Br) to liberate chlorine and bromide radicals in high quantum yield (Φ = 0.76 at 434 nm) upon irradiation with blue light (Figure 6A, top).[6] More recently, Mirica and coworkers demonstrated this reactivity paradigm extends to cationic Ni^{III} dichloride complexes (Figure 6A, bottom).[13] Inspired by these reports, we envisioned halogen atom photoelimination from a cationic Ni^{III} intermediate (**11**) may serve as the halogen atom source in the C–H arylation reaction (Figure 6B). The excited-state reduction potential of photocatalyst **1** (E$_{1/2}$ (Ir^{III*}/Ir^{II}) = 1.21 V)[16] is sufficient to oxidize ($^{t\text{-Bu}}$bpy)Ni^{II}(o-Tol)(Cl) (**3-Cl**) (E$_P$ (Ni^{III}/Ni^{II}) = 0.85 V)[4] to its corresponding cationic Ni^{III} product (**11-Cl**). Blue light irradiation would then liberate free halogen radicals poised to undergo HAT with solvent THF.
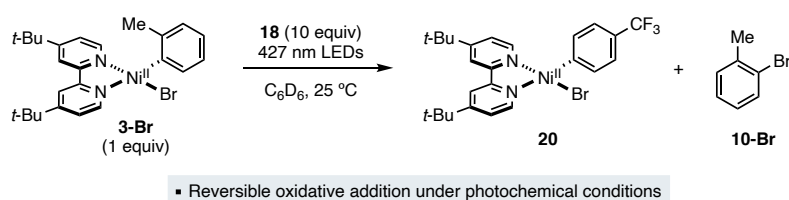
Figure 5. (A) Stoichiometric reactivity of **3** under catalytic conditions with aryl bromide omitted. (B) Crossover aryl bromide experiments. Reactions performed on 0.05 mM scale with dodecane as an internal standard (GC-FID yields). (C) Observing aryl bromide exchange by ^{1}H NMR (4 mM in C$_6$D$_6$, ^{1}H NMR yields with respect to 2-fluorobiphenyl as an internal standard). (D) Proposed mechanism of aryl halide Ni^{II}/Ni^0 cycling.

However, the proposed photochemical reaction from **11-Cl** would have to compete with a potentially rapid C–X reductive elimination, affording aryl halide and Ni^I (Figure 6B). We compute free energy barriers of only 13.4 and 12.1 kcal/mol to the C–X bond forming reductive elimination for chloride and bromides, respectively (**11** → **TS1** → **21**, Figure 7A). In accord with our computations, treatment of **3** with a single electron oxidant ([TBPA]SbCl$_6$, TBPA = tris(4-bromophenyl)ammoniumyl) instantaneously affords stoichiometric yields of the corresponding *o*-Tol halide products (**10**) (see SI).

While such Ni$^{III/I}$ reductive elimination from **11** may prove facile, the resulting Ni^I intermediate may be reduced to Ni^0 (**9**) by ground state Ir^{II} (E$_{1/2}$ (Ir^{III}/Ir^{II}) = –1.37 V versus SCE in MeCN). Rapid ground-state aryl halide oxidative addition to Ni^0 (**9**) affords **3**, which upon SET with the excited-state photocatalyst, regenerates **11**. Hence, under catalytic conditions, a steady-state concentration of **11** may be reached. Given this, we sought to directly evaluate the photochemistry and catalytic relevance of the hypothesized [($^{t\text{-Bu}}$bpy)Ni^{III}(*o*-Tol)(X)]$^+$ intermediate (**11**).

A. Prior art: Facile halogen atom photoelimination from Ni(III)

B. Previously proposed halogen atom generation from cationic Ni(III)

Figure 6. (A) Prior research by Nocera and Mirica demonstrating the feasibility of Ni–X photolysis from Ni(III). (B) Postulated analogous reactivity from a cationic Ni(III) aryl halide intermediate.

For the SET mechanism to be operative, halogen atom photoelimination would need to be more facile than Ni–C(sp²) cleavage. However, our group and others have previously demonstrated (*t*-Bubpy)Ni(II)(*o*-Tol)(X) complexes undergo Ni–C(sp²) homolysis under direct irradiation, albeit in low quantum yield (Φ ~ 2 x 10⁻⁴ at 390 nm).[17] While efficient Ni–X bond homolysis is known from Ni(III),[6,13] to the best of our knowledge, no examples study the selectivity in a complex containing both Ni–X and Ni–C bonds.

To probe this selectivity, we sought to prepare [(*t*-Bubpy)Ni(III)(*o*-Tol)(X)]⁺ complexes (**11**) through in situ oxidation of their Ni(II) precursors (**3**). The photolysis of **11** may yield aryl halide (**3**) from reductive elimination, toluene (**23**) from Ni–C homolysis followed by HAT with THF solvent, or cross-coupled product **8** from Ni–X homolysis and productive cross-coupling. For completeness, we quenched with deuterated trifluoroacetic acid (TFA-*d*) at 25 °C prior to analysis. This labeling allows for distinction between toluene generated from HAT with solvent during photolysis from any remaining Ni–C(sp²) species (*e.g.*, unreacted **3**), which will have deuterium incorporation from deuterodemetalation with TFA-*d*. As a control, **3-Cl** was subjected with these quenching conditions, affording toluene-*d* (**23-d**) with 85% D incorporation.

After establishing photolysis events, we began by examining the competition between thermal reductive elimination and photolysis events from cationic species **11-Cl**. At 25 and 0 °C, reductive elimination prevails, affording aryl chloride **10-Cl** in 80 and 81% yield, respectively (Figure 7B). However, upon further cooling to –40 °C, a more equal partitioning between reductive elimination and Ni–C(sp²) homolysis emerges, with **10-Cl** and toluene (**23**) formed in 52% and 30% (1% D) yield,

respectively. At –78 °C, photolysis outcompetes reductive elimination by an order of magnitude. Here, the cross-coupled product (**8**) is also observed as a minor product (10% yield).

Considering the thermal sensitivity of the cationic Ni(III), we refined our experimental setup to ensure optimal temperature control. To this end, oxidant is introduced to **3-Cl** from a thawing THF solution in a cold bath (at –78 °C). As intended, we find this results in a cleaner reaction profile (see SI). Following this procedure, we sought to evaluate the analogous reactivity from Ni(II) at –78 °C. Omitting light and oxidant from the reaction once again affords toluene in 92% yield (80% D). An indistinguishable result is obtained with irradiation but no oxidant present, indicating no light-induced reactivity of Ni(II) (**3-Cl**) over these short reaction times and reduced temperatures. As before, inclusion of oxidant but omission of light affords **10-Cl** in 89% yield. Treatment of **3-Cl** with oxidant in the presence of irradiation affords predominantly toluene (73% yield, 3% D) with a trace 6% yield of the cross-coupled product **8**. Similar results are obtained from **3-Br** (see SI).

In accord with prior reports by the Nocera and Mirica groups, our oxidation studies highlight that photolysis occurs readily from cationic Ni(III) upon blue light irradiation,[6,13] and with significantly higher quantum yields than their neutral Ni(II) counterparts.[17] However, irradiation of [(*t*-Bubpy)Ni(III)(*o*-Tol)(X)]⁺ complexes (**11**) predominantly leads to Ni–C(sp²) bond homolysis. This is in analogy to the Ni–C over Ni–X homolysis selectivity observed from (*t*-Bubpy)Ni(II)(*o*-Tol)(X) complexes. Given the fate of the *o*-Tol radical as toluene, this process does not represent a step in the productive product-forming catalytic cycle. Thus, we began to investigate an alternative mechanism based in Ir(III)* to Ni triplet energy transfer (³EnT).

Evaluation of a ³EnT-based Mechanism. Recent reports have highlighted the propensity of photocatalyst **1** to undergo ³EnT with related (bpy)Ni(II) complexes.[8,9,12] This is in accord with our conclusion that productive catalysis is not achieved through the SET-based mechanism detailed in Figure 2 (right). Given the likelihood that **1*** is primarily serving as a ³EnT partner, we turned our attention to the energy transfer-based mechanism described in Figure 2 (left).[5] The general hypothesis involves a Ni(0/II) catalytic cycle featuring the intermediacy of a transient Ni(I)(aryl) species (**4**) formed upon Ni–X bond homolysis. This Ni(I)(aryl) intermediate (**4**) captures the THF radical (**5**) to afford a Ni(II)(aryl)(THF) species (**6**), which furnishes the cross-coupled product (**8**) upon reductive elimination.

As this mechanistic paradigm does not involve SET between Ni and Ir catalysts, C–C bond formation is proposed to occur via Ni(II/0) reductive elimination (**6 → 7** in Figure 2). Given the mild reaction conditions (25 °C, 1 h), paired with the challenge of promoting reductive elimination at the Ni(II) oxidation state with a C(sp³) center, we envisioned the C(sp²)–C(sp³) reductive elimination required by this mechanism may not be achievable at a rate relevant to catalysis.[9,18,19] Indeed, local coupled-cluster (DLPNO-CCSD(T))[20] and DFT calculations reveal a free energy barrier of >25 kcal/mol for the C(sp²)–C(sp³) reductive elimination from (*t*-Bubpy)Ni(II)(*o*-Tol)(THF) (**6 → TS2 → 7**, Figure 8). The corresponding rates are in contrast with the reaction kinetics, where catalyst turnover occurs on the minute timescale. Moreover, a rate-limiting reductive elimination from (*t*-Bubpy)Ni(II)(*o*-Tol)(THF) (**6**) offers no explanation as to the substantial rate difference between aryl bromide and chloride electrophiles.

A. Facile Ar–X reductive elimination from [(*t*-Bubpy)Ni^III(*o*-Tol)(X)]^+

X	ΔG‡ (kcal/mol)
Cl	13.4
Br	12.1

■ Cationic Ni^III(*o*-Tol)(X) expected to undergo facile reductive elimination

B. *In situ* oxidation to [(*t*-Bubpy)Ni^III(*o*-Tol)(X)]^+

Effect of temperature

Reaction Temp. (°C)	Yield (%)		
	10-Cl	toluene (23)	8
25	80	4 (n.d.)	0
0	81	3 (n.d.)	0
−40	52	30 (1% D)	0
−78	7	68 (0% D)	10

Photolysis outcompetes reductive elimination at cryogenic temperatures

Role of oxidant and light

Oxidant	Light	Yield (%)		
		10-Cl	toluene (23)	8
yes	no	89	2 (n.d.)	0
yes	yes	1	73 (3% D)	6
no	no	2	92 (80% D)	0
no	yes	1	92 (82% D)	0

Primarily unreacted **3-Cl**

[TBPA]SbCl₆
E_{1/2} = 1.07 V^a
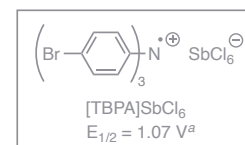
Figure 7. (A) Computational analysis suggests a low barrier to reductive elimination from cationic Ni^III complexes **11-Cl/Br**. Gibbs free energies given in kcal/mol computed at the TPSSh-D4/BS2/CPCM(THF)//PBE-D4/BS1/CPCM(THF) level of theory. See SI for computational details. (B) In situ oxidation studies from **3-Cl**. Reactions carried out under concentrations and equivalencies mirroring that of catalysis (4 mM with respect to Ni in THF). Yields determined by GC-FID with dodecane as an internal standard. Deuterium incorporation determined by GC-MS. See SI for additional details. *a* In MeCN versus SCE.[21]

We then considered whether the halide salt byproducts of the reaction may have a role in promoting reductive elimination from **6**. The bromide anion is known to quench excited-state photocatalyst **1*** affording bromine radical via SET.[22] Radical addition of Br• to **6** would afford (*t*-Bubpy)Ni^III(*o*-Tol)(THF)(Br), which would be well poised to undergo C–C bond formation. Furthermore, the analogous oxidation of chloride to chlorine by **1*** is substantially less favorable (E_{1/2} (Cl⁻/Cl•) = 2.03 V vs SCE in MeCN),[23] possibly explaining the difference in rate between electrophile class. However, addition of exogenous *n*-Bu₄NBr (0.1–1.0 equiv) had no significant effect on the rate of product formation from **10-Cl** (see SI). Thus, we suspect such a process to be either inoperative or a minor contributor to productive catalysis.[15]

Inspired by our findings in the photochemical aryl halide exchange (Figure 5), we then considered whether light could similarly promote C–C bond formation from (*t*-Bubpy)Ni^II(*o*-Tol)(THF) (**6**).[8] An analogous process was hypothesized by Rueping and coworkers in a recent study.[9] To experimentally probe this, we sought to access (*t*-Bubpy)Ni^II(*o*-Tol)(Ns) complex **24** (Ns = neosilyl) as synthetically tractable analog of **6**.[24] Both complexes are computed to have similar ground- and excited-state properties (see SI).

To our delight, transmetalation of **3-Br** with NsMgCl affords **24** as a deep blue crystalline solid in 51% yield. Complex **24** has a half-life of *ca*. 13–24 hours at 25 °C in the dark, slowly decomposing to form C–C coupled product **25** in stoichiometric yield.[25] A barrier to reductive elimination of 24.1 kcal/mol is extrapolated from the first-order decay (see SI for details). This value is in accord with a computed ΔG‡ of 26.0 kcal/mol.

With the model system in hand, we sought to explore the ability of **24** to undergo light-induced reductive elimination. Indeed, irradiation of **24** at 427 nm in the presence of 10 mol% photocatalyst **1** afforded 80% yield of benzyl silane **25** after only 15 minutes.[26] In the absence of photocatalyst, **25** is furnished in 81% yield upon exposure to 427 nm light for 15 minutes. Shorter wavelength light (390 nm) also efficiently promotes C–C bond formation. However diminished reactivity is observed with longer wavelengths of light (467 nm). Multiconfigurational (QD-NEVPT2/CASSCF) and TD-DFT calculations suggest the two absorbance features in the UV-vis spectrum with λ_max of 373 and 586 nm to high- and low-energy MLCT transitions, respectively (see SI).[27] The lack of reactivity upon irradiation into the lower energy MLCT band suggest C–C bond formation occurs from higher energy ³MLCT states.

These same states are also accessed via ^{3}EnT when excited-state photocatalyst is present (**1***) ($E_T \sim 61$ kcal/mol). Additionally, the lack of cross products (biaryl and 1,2-bis(trimethylsilyl)ethane) suggest C–C bond formation does not proceed through a Ni–C homolysis and outer-sphere radical recombination as observed in other systems.[28] In summary, the photochemical conditions of the reaction are capable of promoting C–C bond formation from a Ni^{II}(C(sp^2))(C(sp^3)) intermediate by accessing the appropriate ^{3}MLCT state. While intrigued by these findings, we remained suspect as to whether this photochemical Ni$^{II/0}$ reductive elimination is relevant in actual catalysis.
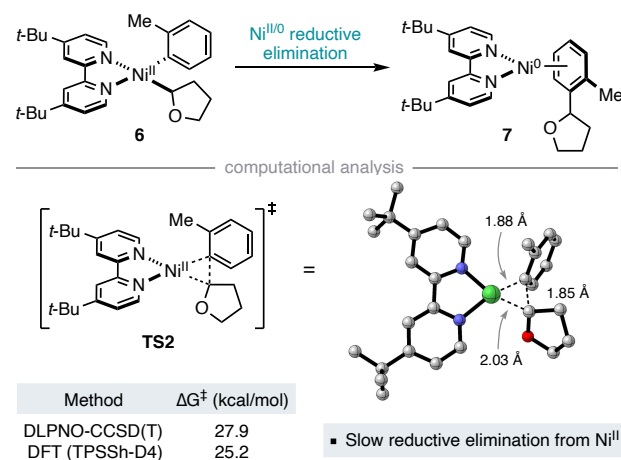
Figure 8. Computed barrier to reductive elimination from **6**. For details on DLPNO-CCSD(T) (TightPNO) and DFT calculations, see SI.

While the transformation of **6** to **7** under photochemical conditions is feasible, analysis of subsequent steps in the mechanism outlined in Figure 2 raises additional questions. One point of contention is the requirement of selective Ni–X homolysis from triplet excited-state Ni^{II} upon ^{3}EnT from Ir^{III*} (**1***). As aforementioned, studies examining excited-state bond homolysis from ($^{t\text{-Bu}}$bpy)Ni^{II}(o-Tol)(X) complexes observe Ni–C(sp^2) homolysis over Ni–X cleavage.[17] While it is possible the ^{3}EnT from Ir^{III*} (**1***) uniquely promotes this selectivity, there is no unambiguous experimental evidence supporting this.[29] Moreover, as mentioned above, exposure of ($^{t\text{-Bu}}$bpy)Ni^{II}(aryl)(X) complexes to Ir^{III*} leads to aryl halide exchange via reductive elimination from a ^{3}MLCT state. The conserved mass balance of these reactions is not consistent with rapid evolution of bromine radicals.

A second issue arises in the postulated selective recombination of the THF radical (**5**) with the transient ($^{t\text{-Bu}}$bpy)Ni^I(aryl) species (**4**). An inner-sphere HAT between X$^•$ and a molecule of THF from the first solvation sphere of **4** is proposed.[30] However, the ability to employ THF, and other unactivated C–H coupling partners such as cyclohexane, in stoichiometric (1–10 equiv) rather than solvent quantities is consistent with an outer-sphere HAT involving cage-escape and diffusion of X$^•$.[31] The organic radical (**5**) generated in this process would likely recombine with ($^{t\text{-Bu}}$bpy)Ni^{II}(o-Tol)(X) (**3**) preferentially over **4** given the orders of magnitude higher concentration of **3** than transient **4**. This rationale also applies to the analogous process between **12** and **13** in the SET-based mechanism highlighted in Figure 2.

In summary, both mechanisms as initially described in Figure 2 are likely incomplete descriptions of the cross-coupling reaction. Selectivity in both halogen atom generation and engagement of the organoradical coupling partner in the Ni catalytic cycle are ill-explained. As such, we sought to explore an updated mechanistic proposal incorporating our new insights.
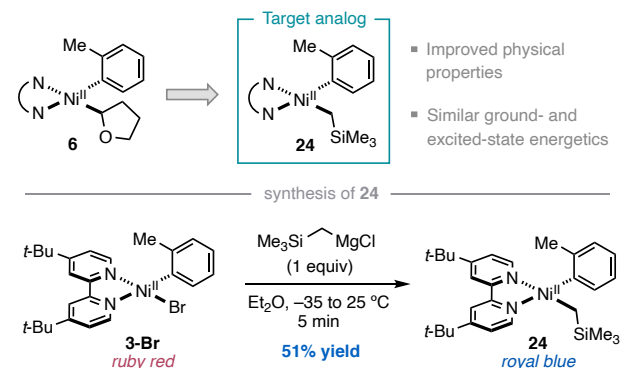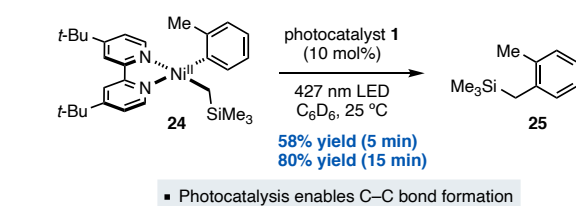
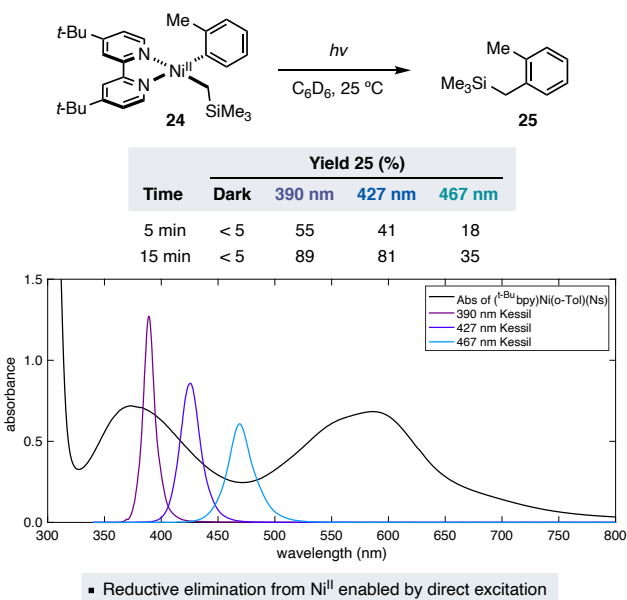**Figure 9.** (A) Synthesis of ($^{t\text{-Bu}}$bpy)Ni^{II}(o-Tol)(Ns) (**24**) from **3-Br**. (B) Rapid C–C bond formation following ^{3}EnT from Ir^{III*}. (C) Observation of light-promoted C–C bond formation in the absence of photocatalyst **1**. Photochemical reactions carried out in C$_6$D$_6$ (1 mM) in J Young tubes with 2-fluorbiphenyl as an internal standard (^{1}H NMR yields). UV-Vis trace of **24** in THF (200 µM).

Alternative proposed mechanism. As mentioned above, the organic radical (**5**) generated via HAT would likely recombine with ($^{t\text{-Bu}}$bpy)Ni^{II}(o-Tol)(X) (**3**) preferentially over any other transient Ni^I intermediate given the orders of magnitude higher

concentration of **3**. From the resultant ($^{t\text{-}Bu}$bpy)Ni^{III}(o-Tol)(THF)(X) species (**29**), a facile C–C bond forming reductive elimination would afford cross-coupled product **8** along with ($^{t\text{-}Bu}$bpy)Ni^{I}X (**26**). Recent experimental[32] and computational[33] studies highlight the energetic feasibility of such a sequence.
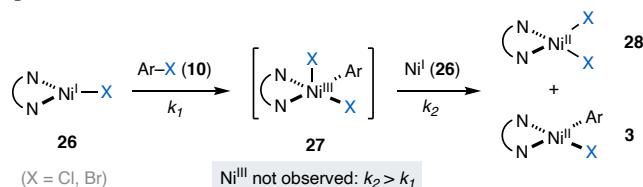

Figure 10. Prior research by Hadt[10] and our group[11] showcasing the oxidative addition of Ni^{I} to aryl chlorides and bromides, followed by rapid comproportionation.

The competency of unactivated aryl chloride coupling partners in the reaction originally led to the assumed intermediacy of Ni^{0} in the prior mechanistic hypotheses. However, recent studies by the Hadt laboratory have demonstrated ($^{t\text{-}Bu}$bpy)Ni^{I}X complexes (**26**) are potent nucleophiles, readily undergoing oxidative addition to even aryl chlorides (Figure 10).[10] Hence, in this context, **26** generated as the product of C–C bond forming reductive elimination, would likely undergo rapid oxidative addition with aryl halide electrophile **10**, forming ($^{t\text{-}Bu}$bpy)Ni^{III}(o-Tol)(X)$_2$ (**27**).

Invoking Ni–X excited-state bond homolysis from **27** would conveniently liberate a halogen radical and regenerate resting state **3**. However, the Ni^{I} oxidative addition studies also highlight the rapid comproportionation between Ni^{I}X (**26**) and Ni^{III}(aryl)(X)$_2$ (**27**) to yield Ni^{II}(aryl)(X) (**3**) and Ni^{II}X$_2$ (**28**), precluding the direct observation of Ni^{III} (**27**). While direct Ni–Br homolysis from **27** cannot be completely ruled out, the rapid

comproportionation renders this process unlikely. In fact, we posited that Ni^{III}/Ni^{I} comproportionation may serve a key role in the prevailing mechanism.

The culmination of these findings leads to our updated mechanistic hypothesis (Figure 11). Photocatalyst **1** can be quenched by either of the Ni^{II} species formed by comproportionation (**3** and **28**). While ^{3}EnT from Ir^{III*} to ($^{t\text{-}Bu}$bpy)Ni^{II}(o-Tol)(X) (**3**) leads to unproductive cycling between **3** and ($^{t\text{-}Bu}$bpy)Ni^{0}(o-TolX) (**9**) (Figure 5D), ^{3}EnT to ($^{t\text{-}Bu}$bpy)Ni^{II}X$_2$ (**28**) has been demonstrated to induce Ni–X homolysis (for X = Cl).[34] Photolysis of **28** serves as the halogen radical source and another source of Ni^{I} halide (**26**). **26** eventually undergoes oxidative addition with aryl halide (**10**) to yield Ni^{III} aryl dihalide **27**, or comproportionates with existing **27** to rapidly afford ($^{t\text{-}Bu}$bpy)Ni^{II}X$_2$ (**28**) and ($^{t\text{-}Bu}$bpy)Ni^{II}(o-Tol)(X) (**3**). Meanwhile, the organic radical coupling partner (**5**) is generated from HAT to the halogen atom. Recombination of **5** with resting-state **3** affords Ni^{III} intermediate **29**, which releases cross-coupled product **8** and Ni^{I}X (**26**) upon reductive elimination, completing the catalytic cycle.

Based on this mechanistic hypothesis, ($^{t\text{-}Bu}$bpy)Ni^{II}X$_2$ (**28**) is a catalytic intermediate from which Ni^{I}X (**26**), **3**, and X$^•$ can arise. Thus, **28-Br** should serve as an effective catalyst in place of **3-Br**. Indeed, employing 10 mol% of **28-Br** under the standard reaction conditions furnishes product **8** in 76% yield after 60 minutes (Figure 12) with a similar k_{obs} to when **3-Br** is employed. Moreover, with **28** as a precatalyst, irradiation (at 370 nm) in the absence of **1** enables sufficient bromide radical generation to achieve catalyst turnover, albeit this process is substantially less efficient than that of ^{3}EnT from **1***. The inefficiency is further compounded in the analogous experiment initiated from **3**, yielding only trace product (Figure 12). ($^{t\text{-}Bu}$bpy)Ni^{II}Cl$_2$ (**28-Cl**) is also a competent precatalyst, with a similar k_{obs} to when employing **3-Cl**.
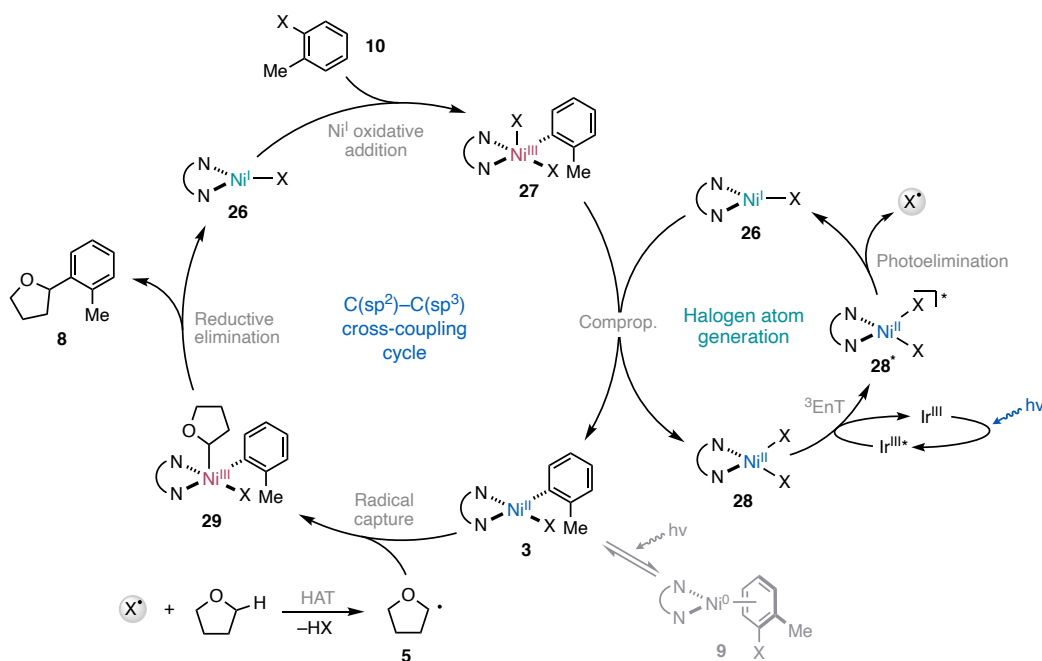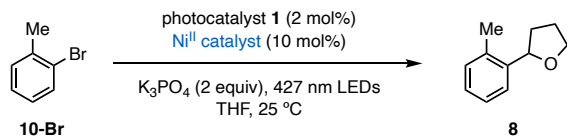

Figure 11. Proposed mechanistic cycle for the Ni-catalyzed photochemical C(sp^3)–H arylation of THF with aryl halide electrophiles.

Figure 12. Competency of various Ni(II) complexes under different photochemical conditions. Reactions performed on 0.05 mM scale with dodecane as an internal standard (GC-FID yields).

Ni(II) catalyst	Deviations from above	Yield (%) 8
(*t-Bu*bpy)NiBr$_2$ (**28-Br**)	none	76 (1 h)
(*t-Bu*bpy)NiBr$_2$ (**28-Br**)	no photocat. **1**	0 (24 h)
(*t-Bu*bpy)NiBr$_2$ (**28-Br**)	no photocat. **1**, 370 nm	26 (24 h)
(*t-Bu*bpy)Ni(*o*-Tol)Br (**3-Br**)	none	79 (1 h)
(*t-Bu*bpy)Ni(*o*-Tol)Br (**3-Br**)	no photocat. **1**	0 (24 h)
(*t-Bu*bpy)Ni(*o*-Tol)Br (**3-Br**)	no photocat. **1**, 370 nm	26 (24 h)
(TMEDA)Ni(*o*-Tol)Br (**30-Br**)	none	53 (5 h)
(*t-Bu*bpy)NiBr$_2$ (**28-Cl**)	none	19 (72 h)

- Both Ni(II)(Ar)(X) and Ni(II)(X)$_2$ are competent precatalysts
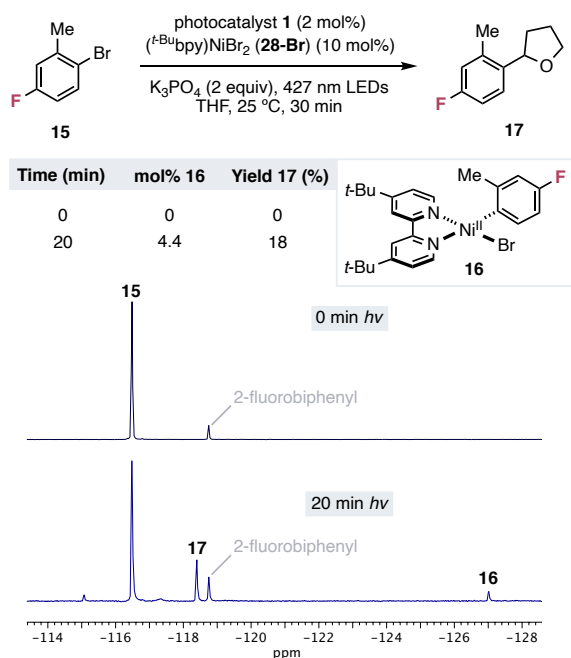
Figure 13. In situ observation ^{19}F NMR of production of **16** from **28-Br**. After 20 min, 44% of Ni resides as **16**. Reaction performed on 0.05 mM scale with 2-fluorobiphenyl as an internal standard (^{19}F NMR yield).

To further probe the hypothesis that Ni(I)Br (**26**) generated by photolysis ultimately yields Ni(II) intermediates **3** and **28**, we returned to in situ reaction monitoring by ^{19}F NMR. In analogy to our aforementioned study (Figure 4), fluorine tagged aryl bromide (**15**) was subject to the standard catalytic conditions now employing **28-Br** as the Ni source. After only 20 minutes of irradiation, the corresponding (*t-Bu*bpy)Ni(II)(4-fluoroaryl)(Br) (**16**) was observed as a 44% fraction of the initially added Ni(II)Br$_2$ (Figure 13). These results highlight the interplay and importance of both Ni(II) intermediates in productive catalysis. Based on our findings, regardless of precatalyst employed, we believe both **3** and **28** will be generated during catalysis (Figures 4 and 13). These two Ni(II) intermediates represent thermodynamic sinks and are each responsible for a key step in catalysis. While the exact partitioning between **3** and **28** is likely governed by several factors, our results suggest both can be present in concentrations of a similar order of magnitude.[35]

2,2'-Bipyridines have served as a privileged ligand class in these transformations. However, our revised mechanistic hypothesis, outlined in Figure 11, does not explicitly rely on bpy-based MLCT states for productive catalysis. To this end, we sought to evaluate the competency of tetramethylethylenediamine (TMEDA) as a redox innocent ligand in place of *t-Bu*bpy. In accord with our hypothesis, (TMEDA)Ni(II)(*o*-Tol)(Br) (**30**) promotes the catalytic transformation, furnishing **8** in 53% yield after 5 hours.

Under this new mechanistic hypothesis, we believe the rate difference observed between aryl chloride and bromide substrate classes arises from an effective rate difference in halogen atom generation from their corresponding Ni(II) dihalide complexes. We envision either a less efficient homolysis process from (*t-Bu*bpy)Ni(II)Cl$_2$ compared to (*t-Bu*bpy)Ni(II)Br$_2$ or a faster recombination between Cl$^{\bullet}$ and (*t-Bu*bpy)Ni(I)Cl to regenerate the Ni(II) dihalide.

In line with studies by our group and others, Ni–C(sp^2) bond homolysis from **3** likely does proceed during the reaction. However, under the reaction conditions the timescales of these photolysis events are much longer than that of the catalytic transformation. Ni–C(sp^2) photolysis may play a role in liberating Ni(I)X to initiate the catalytic cycle when employing **3** as a precatalyst. This may also occur from Ni(I) generation as a byproduct of Ni(0)/Ni(II) comproportionation during the rapid aryl bromide cycling (Figure 5D).

CONCLUSIONS

In summary, we report a comprehensive mechanistic study of a prototypical Ni-catalyzed photochemical C(sp^3)–H arylation reaction. This study revises the previous two general mechanistic paradigms for such transformations.

Through probing the initially-proposed SET-based mechanism, we uncovered the ability of cationic Ni(III) to undergo efficient blue light-induced Ni–C(sp^2) bond homolysis at cryogenic temperatures. At –78ºC, this photolysis outcompetes thermally rapid C–X reductive elimination. While these observations suggest photochemistry from cationic Ni(III) is not relevant to the system under study, these findings may present new opportunities for the generation of reactive intermediates from high-valent Ni.

The ^{3}EnT-based mechanism requires a Ni(II/0) reductive elimination to forge the C–C bond of the cross-coupled product. We find this process is not thermally viably under the catalytic conditions ($\Delta G^{\ddagger} \sim 25$ kcal/mol). However, we find MLCT states of Ni(II)(aryl)(alkyl) complexes, accessed by direct irradiation or ^{3}EnT, efficiently promote C–C bond formation via reductive elimination. Given the assigned (*t-Bu*bpy)Ni(II)(aryl)(X) resting state, the propensity for Ni(II) complexes to capture radical species, and the transiency of (*t-Bu*bpy)Ni(I)(aryl) species, we suspect such Ni(II)(aryl)(alkyl) intermediates are not relevant to the reaction studied herein. However, the ability for direct irradiation to induce bond formation from Ni(II) offers exciting prospects for the development of cross-couplings to form challenging C–C bonds. A photochemical approach to directly enable Ni(II) reductive elimination complements other ground-state-based strategies explored by our group, such as the use of electron-deficient olefins,[36] and redox chemistry.

Our results are most consistent with a new mechanism for the C–H arylation reaction, involving halogen atom evolution from

in situ generated Ni^{II} dihalide intermediates, radical capture by a Ni^{II}(aryl)(halide) resting state, and C–C bond formation through reductive elimination at Ni^{III}. Recent studies highlight the ability of Ni^{I} to undergo rapid oxidative addition with both aryl chlorides and bromides.[10,11] Ni^{I} oxidative addition and rapid downstream Ni^{III}/Ni^{I} comproportionation play key roles in the mechanism. Ni–X bond homolysis from an excited sate of the Ni^{II} dihalide product of this process ultimately serves as the halogen atom source enabling HAT. These results are in accord with recent reports that find similar Ir^{III} photocatalysts preferentially undergo ^{3}EnT with bipyridine Ni^{II} complexes rather than SET.[8,9,12] The insights presented herein not only serve as a platform for development of future C–H cross-coupling reactions, but also offer fundamental insight into the reactivity of Ni in the broader context of catalysis.

ASSOCIATED CONTENT

Supporting Information

The Supporting Information is available free of charge on the ACS Publications website.

Supplementary information (PDF)

Data from quantum mechanics calculations (.xlsx)

Coordinates of computed structures (.zip)

AUTHOR INFORMATION

Corresponding Author

Abigail G. Doyle – Department of Chemistry and Biochemistry, University of California Los Angeles, Los Angeles, California 90095, United States; orcid.org/0000-0002-6641-0833; Email: agdoyle@chem.ucla.edu

Authors

Alexander Q. Cusumano – Department of Chemistry and Biochemistry, University of California Los Angeles, Los Angeles, California 90095, United States; orcid.org/0000-0002-2914-2008; Email: acusuman@chem.ucla.edu
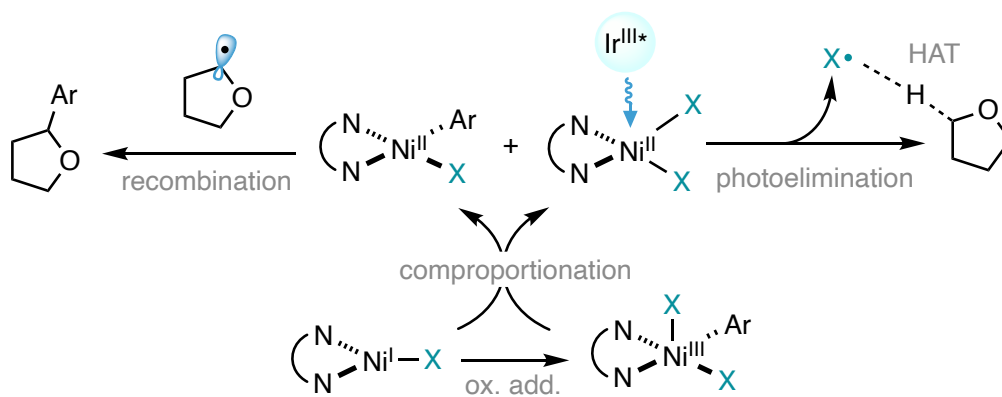
Braden C. Chaffin – Department of Chemistry and Biochemistry, University of California Los Angeles, Los Angeles, California 90095, United States; orcid.org/0009-0002-8378-7453; Email: bchaffin@chem.ucla.edu

Author Contributions

The manuscript was written through contributions of all authors. / All authors have given approval to the final version of the manuscript.

ACKNOWLEDGMENT

References

[1] (a) Chan, A. Y.; Perry, I. B.; Bissonnette, N. B.; Buksh, B. F.; Edwards, G. A.; Frye, L. I.; Garry, O. L.; Lavagnino, M. N.; Li, B. X.; Liang, Y.; Mao, E.; Millet, A.; Oakley, J. V.; Reed, N. L.; Sakai, H. A.; Seath, C. P.; MacMillan, D. W. C. Metal-laphotoredox: The Merger of Photoredox and Transition Metal Catalysis. *Chem. Rev.* **2022**, *122*, 1485–1542. (b) Twilton, J.; Le, C. (Chip); Zhang, P.; Shaw, M. H.; Evans, R. W.; MacMillan, D. W. C. The Merger of Transition Metal and Photocatalysis. *Nat Rev Chem* **2017**, *1*, 1–19. (c) Zuo, Z.; Ahneman, D. T.; Chu, L.; Terrett, J. A.; Doyle, A. G.; MacMillan, D. W. C. Merging Photoredox with Nickel Catalysis: Coupling of α-Carboxyl sp³-Carbons with Aryl Halides. *Science* **2014**, *345*, 437–440.

[2] See select examples of the variety of HAT strategies have emerged in the literature. Using decatungstate catalysis: (a) Perry, I. B.; Brewer, T. F.; Sarver, P. J.; Schultz, D. M.; DiRocco, D. A.; MacMillan, D. W. C. Direct Arylation of Strong Aliphatic C–H Bonds. *Nature* **2018**, *560*, 70–75. Select examples employing quinuclidine HAT catalysts: (b) Le, C.; Liang, Y.; Evans, R. W.; Li, X.; MacMillan, D. W. C. Selective sp³ C–H Alkylation via Polarity-Match-Based Cross-Coupling. *Nature* **2017**, *547*, 79–83. (c) Zhang, X.; MacMillan, D. W. C. Direct Aldehyde C–H Arylation and Alkylation via the Combination of Nickel, Hydrogen Atom Transfer, and Photoredox Catalysis. *J. Am. Chem. Soc.* **2017**, *139*, 11353–11356. Employing perox-ides: (d) Vasilopoulos, A.; Krska, S. W.; Stahl, S. S. C(sp³)–H Methylation Enabled by Peroxide Photosensitization and Ni-Mediated Radical Coupling. *Science* **2021**, *372*, 398–403. For reviews, see: (e) Holmberg-Douglas, N.; Nicewicz, D. A. Pho-toredox-Catalyzed C–H Functionalization Reactions. *Chem. Rev.* **2022**, *122*, 1925–2016. (f) Ye, Z.; Lin, Y.-M.; Gong, L. The Merger of Photocatalyzed Hydrogen Atom Transfer with Transition Metal Catalysis for C−H Functionalization of Alkanes and Cycloalkanes. *Eur. JOC* **2021**, *2021*, 5545–5556.

[3] (a) Kariofillis, S. K.; Doyle, A. G. Synthetic and Mechanistic Implications of Chlorine Photoelimination in Nickel/Photoredox C(sp³)–H Cross-Coupling. *Acc. Chem. Res.* **2021**, *54*, 988–1000. (b) Maity, B.; Dutta, S.; Cavallo, L. The Mechanism of Visible Light-Induced C–C Cross-Coupling by Csp³–H Bond Activation. *Chem. Soc. Rev.* **2023**, *52*, 5373–5387. (c) Yuan, M.; Gutierrez, O. Mechanisms, Challenges, and Opportunities of Dual Ni/Photoredox-Catalyzed C(sp²)–C(sp³) Cross-Couplings. *WIREs Comput Mol Sci* **2022**, *12*, e1573.

[4] Shields, B. J.; Doyle, A. G. Direct C(sp³)–H Cross Coupling Enabled by Catalytic Generation of Chlorine Radicals. *J. Am. Chem. Soc.* **2016**, *138*, 12719–12722.

[5] Heitz, D. R.; Tellis, J. C.; Molander, G. A. Photochemical Nickel-Catalyzed C–H Arylation: Synthetic Scope and Mechanistic Investigations. *J. Am. Chem. Soc.* **2016**, *138*, 12715–12718. Note that a benzophenone additive is sometimes employed in this report, however, the reaction proceeds without the additive.

[6] (a) Hwang, S. J.; Powers, D. C.; Maher, A. G.; Anderson, B. L.; Hadt, R. G.; Zheng, S.-L.; Chen, Y.-S.; Nocera, D. G. Trap-Free Halogen Photoelimination from Mononuclear Ni(III) Complexes. *J. Am. Chem. Soc.* **2015**, *137*, 6472–6475. (b) Hwang, S. J.; Anderson, B. L.; Powers, D. C.; Maher, A. G.; Hadt, R. G.; Nocera, D. G. Halogen Photoelimination from Monomeric Nickel(III) Complexes Enabled by the Secondary Coordination Sphere. *Organometallics* **2015**, *34*, 4766–4774.

[7] (a) Sun, Z.; Kumagai, N.; Shibasaki, M. Photocatalytic α-Acylation of Ethers. *Org. Lett.* **2017**, *19*, 3727–3730. (b) Deng, H.-P.; Fan, X.-Z.; Chen, Z.-H.; Xu, Q.-H.; Wu, J. Photoinduced Nickel-Catalyzed Chemo- and Regioselective Hydroalkylation of Internal Alkynes with Ether and Amide α-Hetero C(sp³)–H Bonds. *J. Am. Chem. Soc.* **2017**, *139*, 13579–13584. (c) Shu, X.;

Huan, L.; Huang, Q.; Huo, H. Direct Enantioselective C(sp^3)–H Acylation for the Synthesis of α-Amino Ketones. *J. Am. Chem. Soc.* **2020**, *142*, 19058–19064. (d) Rand, A. W.; Yin, H.; Xu, L.; Giacoboni, J.; Martin-Montero, R.; Romano, C.; Montgomery, J.; Martin, R. Dual Catalytic Platform for Enabling sp^3 α C–H Arylation and Alkylation of Benzamides. *ACS Catal.* **2020**, *10*, 4671–4676. (e) Cheng, X.; Lu, H.; Lu, Z. Enantioselective Benzylic C–H Arylation via Photoredox and Nickel Dual Catalysis. *Nat Commun* **2019**, *10*, 3549. (f) Shu, X.; Zhong, D.; Lin, Y.; Qin, X.; Huo, H. Modular Access to Chiral α-(Hetero)Aryl Amines via Ni/Photoredox-Catalyzed Enantioselective Cross-Coupling. *J. Am. Chem. Soc.* **2022**, *144*, 8797–8806. (g) Huan, L.; Shu, X.; Zu, W.; Zhong, D.; Huo, H. Asymmetric Benzylic C(sp^3)−H Acylation via Dual Nickel and Photoredox Catalysis. *Nat Commun* **2021**, *12*, 3536. (h) Cheng, X.; Li, T.; Liu, Y.; Lu, Z. Stereo- and Enantioselective Benzylic C–H Alkenylation via Photoredox/Nickel Dual Catalysis. *ACS Catal.* **2021**, *11*, 11059–11065. (i) Xu, J.; Li, Z.; Xu, Y.; Shu, X.; Huo, H. Stereo-divergent Synthesis of Both Z- and E-Alkenes by Photoinduced, Ni-Catalyzed Enantioselective C(sp^3)–H Alkenylation. *ACS Catal.* **2021**, *11*, 13567–13574. (j) Shen, Y.; Gu, Y.; Martin, R. sp^3 C–H Arylation and Alkylation Enabled by the Synergy of Triplet Excited Ketones and Nickel Catalysts. *J. Am. Chem. Soc.* **2018**, *140*, 12200–12209. (j) Xu, S.; Ping, Y.; Li, W.; Guo, H.; Su, Y.; Li, Z.; Wang, M.; Kong, W. Enantioselective C(sp^3)–H Functionalization of Oxacycles via Photo-HAT/Nickel Dual Catalysis. *J. Am. Chem. Soc.* **2023**, *145*, 5231–5241. (k) Santos, M. S.; Corrêa, A. G.; Paixão, M. W.; König, B. C(sp^3)−C(sp^3) Cross-Coupling of Alkyl Bromides and Ethers Mediated by Metal and Visible Light Photoredox Catalysis. *Adv. Synth. Catal.* **2020**, *362*, 2367–2372. (l) Huang, L.; Rueping, M. Direct Cross-Coupling of Allylic C(sp^3)−H Bonds with Aryl- and Vinylbromides by Combined Nickel and Visible-Light Catalysis. *Angew. Chem. Int. Ed.* **2018**, *57*, 10333–10337. (m) Ackerman, L. K. G.; Martinez Alvarado, J. I.; Doyle, A. G. Direct C–C Bond Formation from Alkanes Using Ni-Photoredox Catalysis. *J. Am. Chem. Soc.* **2018**, *140*, 14059–14063. (n) Nielsen, M. K.; Shields, B. J.; Liu, J.; Williams, M. J.; Zacuto, M. J.; Doyle, A. G. Mild, Redox-Neutral Formylation of Aryl Chlorides through the Photocatalytic Generation of Chlorine Radicals. *Angew. Chem. Int. Ed.* **2017**, *129*, 7297–7300.

[8] In the context of C–O bond formation from bipyridine Ni^{II} aryl acetates: (a) Welin, E. R.; Le, C.; Arias-Rotondo, D. M.; McCusker, J. K.; MacMillan, D. W. C. Photosensitized, Energy Transfer-Mediated Organometallic Catalysis through Electronically Excited Nickel(II). *Science* **2017**, *355*, 380–385. (b) Tian, L.; Till, N. A.; Kudisch, B.; MacMillan, D. W. C.; Scholes, G. D. Transient Absorption Spectroscopy Offers Mechanistic Insights for an Iridium/Nickel-Catalyzed C–O Coupling. *J. Am. Chem. Soc.* **2020**, *142*, 4555–4559. For computational evaluation of C–O bond forming reductive elimination from the ^{3}MLCT state, see (c) Ma, P.; Wang, S.; Chen, H. Reactivity of Transition-Metal Complexes in Excited States: C–O Bond Coupling Reductive Elimination of a Ni(II) Complex Is Elicited by the Metal-to-Ligand Charge Transfer State. *ACS Catal.* **2020**, *10*, 1–6.

[9] Kancherla, R.; Muralirajan, K.; Maity, B.; Karuthedath, S.; Kumar, G. S.; Laquai, F.; Cavallo, L.; Rueping, M. Mechanistic Insights into Photochemical Nickel-Catalyzed Cross-Couplings Enabled by Energy Transfer. *Nat Commun* **2022**, *13*, 2737.

[10] Cagan, D. A.; Bím, D.; McNicholas, B. J.; Kazmierczak, N. P.; Oyala, P. H.; Hadt, R. G. Photogenerated Ni(I)–Bipyridine Halide Complexes: Structure–Function Relationships for Competitive C(sp^2)–Cl Oxidative Addition and Dimerization Reactivity Pathways. *Inorg. Chem.* **2023**, *62*, 9538–9551.

[11] (a) Newman-Stonebraker, S. H.; Raab, T. J.; Roshandel, H.; Doyle, A. G. Synthesis of Nickel(I)–Bromide Complexes via Oxidation and Ligand Displacement: Evaluation of Ligand Effects on Speciation and Reactivity. *J. Am. Chem. Soc.* **2023**, *145*, 19368–19377. (b) Ting, S. I.; Williams, W. L.; Doyle, A. G. Oxidative Addition of Aryl Halides to a Ni(I)-Bipyridine Complex. *J. Am. Chem. Soc.* **2022**, *144*, 5575–5582.

[12] Kudisch, M.; Lim, C.-H.; Thordarson, P.; Miyake, G. M. Energy Transfer to Ni-Amine Complexes in Dual Catalytic, Light-Driven C–N Cross-Coupling Reactions. *J. Am. Chem. Soc.* **2019**, *141*, 19479–19486.

[13] Na, H.; Watson, M. B.; Tang, F.; Rath, N. P.; Mirica, L. M. Photoreductive Chlorine Elimination from a Ni(III)Cl$_2$ Complex Supported by a Tetradentate Pyridinophane Ligand. *Chem. Commun.* **2021**, *57*, 7264–7267.

[14] Burés, J. Variable Time Normalization Analysis: General Graphical Elucidation of Reaction Orders from Concentration Profiles. *Angew. Chem. Int. Ed.* **2016**, *55*, 16084–16087.

[15] Ben-Tal, Y.; Lloyd-Jones, G. C. Kinetics of a Ni/Ir-Photocatalyzed Coupling of ArBr with RBr: Intermediacy of ArNi^{II}(L)Br and Rate/Selectivity Factors. *J. Am. Chem. Soc.* **2022**, *144*, 15372–15382.

[16] In MeCN versus SCE. Lowry, M. S.; Goldsmith, J. I.; Slinker, J. D.; Rohl, R.; Pascal, R. A.; Malliaras, G. G.; Bernhard, S. Single-Layer Electroluminescent Devices and Photoinduced Hydrogen Production from an Ionic Iridium(III) Complex. *Chem. Mater.* **2005**, *17* (23), 5712–5719.

[17] (a) Ting, S. I.; Garakyaraghi, S.; Taliaferro, C. M.; Shields, B. J.; Scholes, G. D.; Castellano, F. N.; Doyle, A. G. 3d-d Excited States of Ni(II) Complexes Relevant to Photoredox Catalysis: Spectroscopic Identification and Mechanistic Implications. *J. Am. Chem. Soc.* **2020**, *142*, 5800–5810. (b) Cagan, D. A.; Bím, D.; Silva, B.; Kazmierczak, N. P.; McNicholas, B. J.; Hadt, R. G. Elucidating the Mechanism of Excited-State Bond Homolysis in Nickel–Bipyridine Photoredox Catalysts. *J. Am. Chem. Soc.* **2022**, *144*, 6516–6531. (c) Cagan, D. A.; Stroscio, G. D.; Cusumano, A. Q.; Hadt, R. G. Multireference Description of Nickel–Aryl Homolytic Bond Dissociation Processes in Photoredox Catalysis. *J. Phys. Chem. A* **2020**, *124*, 9915–9922.

[18] (a) Matsunaga, P. T.; Hillhouse, G. L.; Rheingold, A. L. Oxygen-Atom Transfer from Nitrous Oxide to a Nickel Metallacycle. Synthesis, Structure, and Reactions of [Cyclic] (2,2'-Bipyridine)Ni(OCH$_2$CH$_2$CH$_2$CH$_2$). *J. Am. Chem. Soc.* **1993**, *115*, 2075–2077. (b) Han, R.; Hillhouse, G. L. Carbon−Oxygen Reductive-Elimination from Nickel(II) Oxametallacycles and Factors That Control Formation of Ether, Aldehyde, Alcohol, or Ester Products. *J. Am. Chem. Soc.* **1997**, *119*, 8135–8136. (c) Le Vaillant, F.; Reijerse, E. J.; Leutzsch, M.; Cornella, J. Dialkyl Ether Formation at High-Valent Nickel. *J. Am. Chem. Soc.* **2020**, *142*, 19540–19550. (d) Lohrey, T. D.; Cusumano, A. Q.; Goddard, W. A. I.; Stoltz, B. M. Identifying the Imperative Role of Metal–Olefin Interactions in Catalytic C–O Reductive Elimination from Nickel(II). *ACS Catal.* **2021**, *11*, 10208–10222. For an example of promoting Ni(II) C–O reductive elimination via ligand design, see: (e) MacQueen, P. M.; Tassone, J. P.; Diaz, C.; Stradiotto, M. Exploiting Ancillary Ligation To Enable Nickel-Catalyzed C–O Cross-Couplings of Aryl Electrophiles with Aliphatic Alcohols. *J. Am. Chem. Soc.* **2018**, *140*, 5023–5027.

[19] Dong, Y.-J.; Zhao, Z.-W.; Geng, Y.; Su, Z.-M.; Zhu, B.; Guan, W. Theoretical Insight on the High Reactivity of Reductive Elimination of Ni^{III} Based on Energy- and Electron-Transfer Mechanisms. *Inorg. Chem.* **2023**, *62*, 1156–1164.

[20] (a) Neese, F. Software Update: The ORCA Program System─Version 5.0. *WIREs Comput. Mol. Sci.* **2022**, *12*, e1606. (b) Riplinger, C.; Neese, F. An Efficient and near Linear Scaling Pair Natural Orbital Based Local Coupled Cluster Method. *J. Chem. Phys.* **2013**, *138*, 034106. (c) Riplinger, C.; Sandhoefer, B.; Hansen, A.; Neese, F. Natural Triple Excitations in Local Coupled Cluster Calculations with Pair Natural Orbitals. *J. Chem. Phys.* **2013**, *139*, 134101. (d) Riplinger, C.; Pinski, P.; Becker, U.; Valeev, E. F.; Neese, F. Sparse Maps—A Systematic Infrastructure for Reduced-Scaling Electronic Structure Methods. II. Linear Scaling Domain Based Pair Natural Orbital Coupled Cluster Theory. *J. Chem. Phys.* **2016**, *144*, 024109.

[21] Connelly, N. G.; Geiger, W. E. Chemical Redox Agents for Organometallic Chemistry. *Chem. Rev.* **1996**, *96*, 877–910.

[22] See supporting information: (a) Zhang, P.; Le, C. "Chip"; MacMillan, D. W. C. Silyl Radical Activation of Alkyl Halides in Metallaphotoredox Catalysis: A Unique Pathway for Cross-Electrophile Coupling. *J. Am. Chem. Soc.* **2016**, *138*, 8084–8087. (b) Rand, A. W.; Chen, M.; Montgomery, J. Investigations into Mechanism and Origin of Regioselectivity in the Metallaphotoredox-Catalyzed α-Arylation of N-Alkylbenzamides. *Chem. Sci.* **2022**, *13*, 10566–10573.

[23] Isse, A. A.; Lin, C. Y.; Coote, M. L.; Gennaro, A. Estimation of Standard Reduction Potentials of Halogen Atoms and Alkyl Halides. *J. Phys. Chem. B* **2011**, *115*, 678–684.

[24] Ju, L.; Lin, Q.; LiBretto, N. J.; Wagner, C. L.; Hu, C. T.; Miller, J. T.; Diao, T. Reactivity of (Bi-Oxazoline)Organonickel Complexes and Revision of a Catalytic Mechanism. *J. Am. Chem. Soc.* **2021**, *143*, 14458–14463.

[25] The rate of C–C bond forming reductive elimination is ligand dependent. Yamamoto reports a first-order rate constant of 1 x 10^{-4} s^{-1} for reductive elimination from 1,2-Bis(dimethylphosphino)ethane (dmpe) complex (dmpe)Ni(*o*-Tol)(Me) at 30 ºC. Komiya, S.; Abe, Y.; Yamamoto, A.; Yamamoto, T. Phosphine-Induced Reductive Elimination from Cis-Arylmethylnickel(II) Complexes Having a 1,2-Bis(Dimethylphosphino)Ethane Ligand. *Organometallics* **1983**, *2*, 1466–1468.

[26] The Diao group reports similar reactivity from a (BiOx)Ni(Ns)$_2$ in the presence of **1** upon irradiation for 1 hour with blue LEDs in C$_6$D$_6$. Reductive elimination was attributed to the oxidation of (BiOx)Ni(Ns)$_2$ by **1**; however, in light of our findings this may also arise from ^{3}MLCT reactivity. Ju, L.; Hu, C. T.; Diao, T. Strategies for Promoting Reductive Elimination of Bi- and Bis-Oxazoline Ligated Organonickel Complexes. *Organometallics* **2022**, *41*, 1748–1753.

[27] Similar features were observed in the UV-Vis spectrum of (*t*-Bubpy)NiMe$_2$. Yamaguchi, Y.; Ichioka, H.; Klein, A.; Brennessel, W. W.; Vicic, D. A. Linear Bis(Perfluoroalkyl) Complexes of Nickel Bipyridine. *Organometallics* **2012**, *31*, 1477–1483. See also reference 28a.

[28] (a) Shin, J.; Lee, J.; Suh, J.-M.; Park, K. Ligand-Field Transition-Induced C–S Bond Formation from Nickelacycles. *Chem. Sci.* **2021**, *12*, 15908–15915. (b) Oderinde, M. S.; Jin, S.; Das, J.; Jorge, C.; Yip, S.; Ramirez, A.; Wu, D.-R.; Li, Y.; Kempson, J.; Meanwell, N. A.; Mathur, A.; Dhar, T. G. M. Photo-Initiated Nickel Catalysis (PiNiC): Unmasking Dimethylnickel with Light. *ACS Catal.* **2022**, *12*, 12511–12520.

[29] While no direct experimental evidence has this far demonstrated Ni–X over Ni–C(sp^2) homolysis selectivity, a computational study by Cavallo and Gagliardi suggest Ni–Br homolysis from (bpy)Ni(Ph)(Br) is possible. Maity, B.; Scott, T. R.; Stroscio,

G. D.; Gagliardi, L.; Cavallo, L. The Role of Excited States of LNi[II/III](Aryl)(Halide) Complexes in Ni–Halide Bond Homolysis in the Arylation of Csp[3]–H Bonds. *ACS Catal.* **2022**, *12*, 13215–13224. Studies by Reuping and coworkers (reference 9) highlight the formation of a Ni[I] species upon [3]EnT, however this may also correspond to Ni[I]–Br as observed by Hadt and coworkers and Doyle and coworkers (references 17a–b).

[30] Prior studies suggest a more direct C–H activation mechanism involving Ni to not be operative. See reference 7j. An alternative CMD was proposed by Chen and coworkers from valence inverted states of Ni. Wang, S.; Ma, P.; Shaik, S.; Chen, H. Valence-Inverted States of Nickel(II) Complexes Perform Facile C–H Bond Activation. *J. Am. Chem. Soc.* **2022**, *144*, 14607–14613. This study also finds direct σ metathesis unlikely. However, the proposed mechanism may not agree with findings of Martin *et. al.* that a 2,5-dimethyltetrahydrofuran as a 1:1 cis/trans mixture undergoes arylation to afford a single diastereomer of product. Moreover, the reaction studied herein proceeds readily with the redox innocent TMEDA ligand.

[31] In related systems, the regioselectivity of HAT between primary, secondar, and tertiary centers is in accord with free halogen atom HAT (see reference 7m–n).

[32] (a) Lin, Q.; Spielvogel, E. H.; Diao, T. Carbon-Centered Radical Capture at Nickel(II) Complexes: Spectroscopic Evidence, Rates, and Selectivity. *Chem* **2023**, *9*, 1295–1308. (b) Wei, Y.; Ben-zvi, B.; Diao, T. Diastereoselective Synthesis of Aryl C-Glycosides from Glycosyl Esters via C−O Bond Homolysis. *Angew. Chem. Int. Ed.* **2021**, *60*, 9433–9438.

[33] Sanosa, N.; Ruiz-Campos, P.; Ambrosi, D.; Sampedro, D.; Funes-Ardoiz, I. Investigating the Mechanism of Ni-Catalyzed Coupling of Photoredox-Generated Alkyl Radicals and Aryl Bromides: A Computational Study. *Int. J. Mol. Sci.* **2023**, *24*, 9145.

[34] Zieleniewska, A.; Earley, J.; Yu, J.; Kudisch, M.; DiLuzio, S.; Cordones, A.; Sayre, H.; Zhang, X.; Rumbles, G.; Reid, O., Tetrahedral to Octahedral Nickel(II) as an Initiation Step in Metallaphotoredox Catalysis. doi.org/10.26434/chemrxiv-2023-wptwr-v2.

[35] Diao has found similar partitioning between (phen)NiBr$_2$ and (phen)Ni(Ph)(Br) in the mechanism of Ni-catalyzed reductive alkene difunctionalization. Lin, Q.; Diao, T. Mechanism of Ni-Catalyzed Reductive 1,2-Dicarbofunctionalization of Alkenes. *J. Am. Chem. Soc.* **2019**, *141*, 17937–17948.

[36] (a) Huang, C.-Y. (Dennis); Doyle, A. G. Electron-Deficient Olefin Ligands Enable Generation of Quaternary Carbons by Ni-Catalyzed Cross-Coupling. *J. Am. Chem. Soc.* **2015**, *137*, 5638–5641. (b) Estrada, J. G.; Williams, W. L.; Ting, S. I.; Doyle, A. G. Role of Electron-Deficient Olefin Ligands in a Ni-Catalyzed Aziridine Cross-Coupling to Generate Quaternary Carbons. *J. Am. Chem. Soc.* **2020**, *142*, 8928–8937.